Electrodeposition of PdAu Alloy Nanoparticles on Ionic Liquid Functionalized Graphene Film for the Voltammetric Determination of Oxalic Acid

Lei Shang, Faqiong Zhao, Baizhao Zeng*

The Key Laboratory of Analytical Chemistry for Biology and Medicine (Ministry of Education), College of Chemistry and Molecular Sciences, Wuhan University, Wuhan 430072, Hubei Province, P. R. China
tel: +086-27-68752701, fax: 086-27-68754067
*e-mail: fqzhao@whu.edu.cn

Received: October 8, 2012
Accepted: November 10, 2012
Published online: ■■ ■■, 0000

Abstract
An ionic liquid functionalized graphene film was prepared and PdAu nanoparticles (NPs) were electrodeposited on it. The PdAu NPs were characterized by various methods and they showed the features of alloys. In 0.2 M H_2SO_4 solution, oxalic acid (OA) exhibited a sensitive anodic peak at the resulting electrode at about 1.1 V (vs. SCE), and the peak current was linear to OA concentration in the range of 5–100 μM with a sensitivity of 45.5 μA/mM. The detection limit was 2.7 μM ($S/N=3$). The electrode was successfully applied to the determination of OA in real sample.

Keywords: PdAu nanoparticle, Graphene, Electrodeposition, Oxalic acid, Ionic liquid

DOI: 10.1002/elan.201200540

Supporting Information for this article is available on the WWW under http://dx.doi.org/10.1002/elan.201200540

1 Introduction

Oxalic acid (OA) easily interacts with Ca^{2+} and Mg^{2+} to form insoluble salts, thus excess ingestion of OA can lead to the injury of the kidneys [1,2]. Therefore, the detection of OA in foods is significant. Various methods have been reported for the determination of OA, such as spectrophotometry [3], chromatography [4,5], ion exclusion chromatography [6] and enzymatic method [7,8]. However, these methods still show some disadvantages, such as low sensitivity and/or low selectivity [3–7]. Electroanalytical methods are generally simple and sensitive, and some researchers expected them to show good performance in the determination of OA and performed them [9–11]. For example, Zheng et al. used a carbon nanotube modified electrode to determine OA. It presented a linear response in the range from 5.0×10^{-5} M to 1.5×10^{-2} M and a detection limit of 1.20×10^{-5} M [10]. Arguello et al. prepared a cobalt phthalocyanine bulk-modified carbon ceramic composite electrode for the detection of OA and a linear response was observed in the range from 1.6×10^{-5} M–1.5×10^{-3} M [11]. The detection limit was 7.1 μM. The electroanalytical methods for OA are generally based on the electrochemical oxidation of OA.

Pd and Au showed catalysis to the electrochemical oxidation of OA [12–15]. For example, Casella et al. investigated the electrocatalytic oxidation of OA at a Pd modified electrode in $HClO_4$ solutions and they thought that two independent electrooxidation processes occurred [12]. A Pd nanoparticle-loaded carbon nanofiber (Pd/CNF) was prepared and applied to the determination of OA in spinach [13], but the detection limit was as high as 0.2 mM. Haber et al. found that a gold coated vanadium-TiO_2/Ti electrode exhibited high electrocatalytic activity and antipoisoning power towards OA [15]. However, so far PdAu alloy nanoparticles have not been used for OA detection. It is well known that in many cases alloy nanoparticles show improved physical and chemical properties due to the synergistic effects of monometals [16]. Therefore, PdAu alloy is expected to present high electrocatalysis to OA.

Graphene has drawn worldwide attention as it has large specific surface area and high-speed electron mobility etc. [17,18]. When metal nanoparticles are loaded on graphene sheets the resulted metal-graphene hybrid has a large active surface and good electron-transport property, which was confirmed to be useful in constructing electrochemical sensors [19–22]. Graphene is generally prepared through chemical reduction, but it can also be prepared by electrochemical reduction. Furthermore, it was reported that the graphene prepared by electrochemical reduction displayed better properties [23–26]. In addition, alloy nanoparticles can be fabricated by convenient and controllable electrodeposition methods. Therefore, alloy-

graphene hybrid can be prepared by using facile electrochemical methods.

Herein, graphene oxide (GO) and ionic liquid (IL) 1-(2-hydroxyethyl)-3-methylimidazolium bis(trifluoromethanesulfonyl)imide ([HeMIM][NTf_2]) are mixed and then the mixture is transferred on a glassy carbon electrode (GCE). After it is reduced electrochemically PdAu nanoparticles are electrodeposited on it. The structural and electrochemical properties of PdAu nanoparticles are studied using scanning electron microscopy (SEM), energy dispersive X-ray spectroscopy (EDX), X-ray diffraction (XRD) and voltammetry. It is found that the resulted electrode exhibits high catalytic activity toward the electrooxidation of OA, and it has good application potential in OA detection.

2 Experimental

2.1 Reagents

$HAuCl_4$ and $PdCl_2$ were purchased from Sinopharm Chemical Reagent Co. Ltd. (Shanghai, China). The [HeMIM][NTf_2] (purity: 99%) was provided by Lanzhou Institute of Chemical Physics (Lanzhou, China) and used as received. The GO came from Xianfeng Reagent Co. Ltd. (Nanjing, China). The OA was the product of Sinopharm Chemical Reagent Co. Ltd. (Shanghai, China), and its stock solution (0.5 M) was prepared with water and stored in a refrigerator. The working solutions were prepared by diluting the stock solution with 0.2 M H_2SO_4. All other chemicals used were of analytical reagent grade. The water used was redistilled.

2.2 Apparatus

Electrodeposition and cyclic voltammetric experiments were performed with a CHI 440 electrochemical workstation (CH Instrument Company, Shanghai, China). A conventional three-electrode system was adopted. The working electrode was a modified GCE (diameter: 2 mm) or a glass substrate (10 mm × 10 mm × 2.2 mm) coated with indium tin oxide (ITO), and the auxiliary and reference electrodes were a platinum wire and a saturated calomel electrode (SCE), respectively. Fourier transform infrared (FTIR) absorption spectra were recorded with a model Nexus-670 spectrometer (Nicolet, USA). The SEM images and EDX were obtained using a Hitachi X-650 SEM (Hitachi Co., Japan). The XRD data were recorded with a Bruke D8 diffractometer (Germany) using Cu Kα radiation (40 kV, 40 mA) with a Ni filter. All measurements were conducted at room temperature.

2.3 Preparation of Spinach Sample

The spinach sample was pretreated as mentioned in the literature [27]. Briefly, 4 g spinach (from a local market) was cut into small pieces and refluxed in water for 50 min. The suspension was centrifuged at 3000 rpm for 3 min. The supernatant was filtered with $\varnothing = 0.45$ μm filter film and then diluted to 60 mL.

2.4 Preparation of PdAu Nanoparticle Modified Electrodes

The exfoliated GO was achieved by ultrasonication in redistilled water and 1 mg/mL GO brown suspension was obtained. Then 0.5 mL of this brown suspension was mixed with 0.5 mL *N*,*N*-dimethylformamide (DMF) containing 2.5 μL IL, with the aid of ultrasonication. After that 4 μL of the resulted suspension was transferred onto a cleaned GCE and the solvent was evaporated in air; thus an IL-GO film coated electrode (i.e. GO-IL/GCE) was obtained. The electrochemical reduction of GO-IL/GCE was performed in 0.2 M Na_2SO_4 aqueous solution for 600 s at −1.3 V (vs. SCE). In this case, GO was electrochemically reduced to graphene (EGN) and the resulting electrode was denoted as EGN-IL/GCE. PdAu nanoparticles were electrodeposited on the surface of EGN-IL/GCE at −0.2 V for 200 s. The electrolyte solution was 0.5 M H_2SO_4 aqueous solution plus 1.33 mM $HAuCl_4$ and 0.67 mM $PdCl_2$. The obtained $PdAu_2$ (1:2, i.e., the ratio of $c(PdCl_2)/c(HAuCl_4)$)–EGN-IL/GCE (or ITO) was washed carefully with redistilled water and then dried at room temperature. For comparison, $PdAu_2$/GCE (or ITO), Au–EGN-IL/GCE (or ITO) and Pd–EGN-IL/GCE (or ITO) were fabricated through the similar method. Before measurement, the working electrode was conditioned by repeating potential scan (e.g. for 6 times) between 0.6 V and 1.3 V in a 0.2 M H_2SO_4 until a stable CV curve was obtained.

3 Results and Discussion

3.1 Morphological Analysis

As shown in Figure 1, the obtained EGN film presents the typical wrinkled sheet structure of graphene [26]. But the EGN-IL composite film is quite uniform. This can be attributed to the binding and blanketing effect of IL. After the electrodeposition of PdAu dense particles can be observed on the EGN-IL composite film. The particles are well dispersed and the particle diameter is about 60 nm. However, when the EGN-IL/ITO is replaced by EGN/ITO, the electrodeposited particles become big and the particle density decreases. At ITO the electrodeposited particles are bigger and the particle density is lower. This indicates that both EGN and IL can promote the electrodeposition of small PdAu particles. The reason is that EGN can provide a large number of nucleation sites due to its large surface. In addition, IL has low interface tension, leading to high nucleation rate [28], and it can also block the aggregation of PdAu nanoparticles.

It should be pointed out, that the imidazolium and hydroxyl groups of this IL can interact with GO and promote its dispersion [29–31]. Meanwhile, the IL can form a hydrophobic area outside the PdAu particles and act as

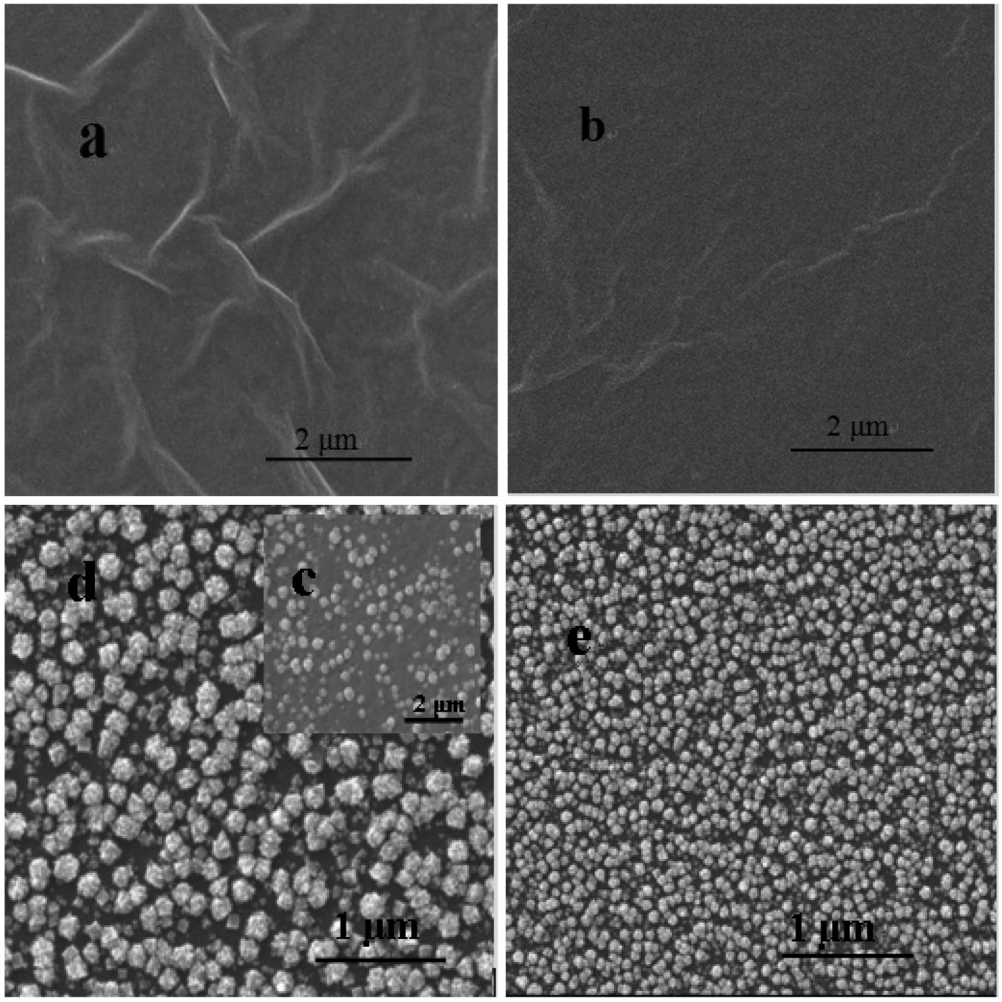

Fig. 1. SEM images of EGN/ITO (a), EGN-IL/ITO (b), $PdAu_2$/ITO (c), $PdAu_2$-EGN /ITO (d), and $PdAu_2$-EGN-IL/ITO (e). The solution composition for electrodeposition: 0.2 M H_2SO_4 containing 1.33 mM $HAuCl_4$ and 0.67 mM $PdCl_2$; electrodeposition potential: −0.2 V; electrodeposition time: 200 s.

a stable reagent. These benefit the preparation of PdAu-EGN-IL, thus the IL is selected among several ILs.

As to the formation of EGN, this can be confirmed by FTIR spectra (Supplementary Materials, Figure S1). GO shows absorption bands at 1059, 1395, 1740 and 3200 cm^{-1}, belonging to the oxygen-containing groups (–OH, C–O–C on the plane and –COOH on the edge) [23]. After it is reduced, these bands disappear or become considerably weak, indicating the formation of EGN. When IL is introduced, the band of C=C shifts a little and some new peaks of IL are observed.

3.2 Structure and Composition Analysis

Figure 2 shows the XRD patterns of Au, Pd and $PdAu_2$ particles electrodeposited. The peaks around 38.18°, 44.38°, 64.67° and 77.71° can be assigned to Au (111), (200), (220) and (311) (JCPDS 04-0784), respectively. And the peaks at 40.12°, 46.66°, and 68.08° belong to Pd (111), (200) and (220), according to the powder diffrac-

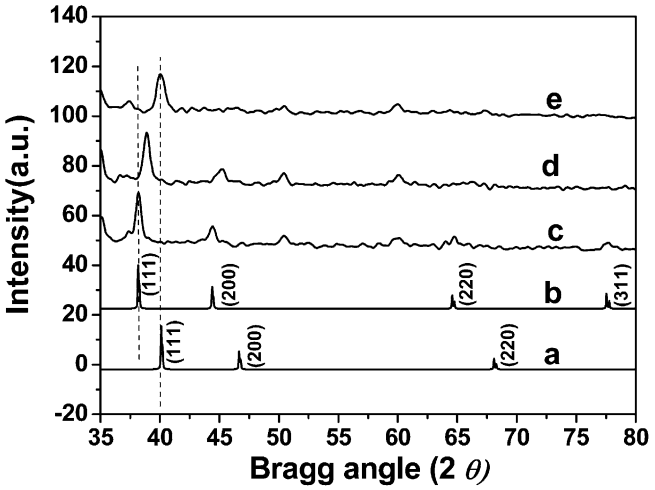

Fig. 2. Standard XRD patterns of Pd (a) and Au (b); XRD patterns of Au (c), $PdAu_2$ (d), and Pd (e) particles electrodeposited on EGN-IL film.

tion standard data (JCPDS 05-0681). The peaks around 50° and 60° are produced by ITO.

In order to compare the diffraction peaks of different nanoparticles, part of the XRD patterns are enlarged (Supporting Information, Fig. S2). Obviously, the peak of the crystal face (111) of $PdAu_2$ nanoparticles locates between the corresponding peaks of Au-EGN-IL and Pd-EGN-IL, indicating that the $PdAu_2$ nanoparticles are alloy rather than the mixture of monometallic nanoparticles. As Pd atom has smaller radii than Au atom, its incorporation causes the shrinkage of lattice parameter, resulting in the peak shift. Assuming the validity of Vegard's Law (the linear lattice constant – concentration relation) [32,33], the Pd/Au ratio of the alloy can be estimated to be 34:66.

The composition of $PdAu_2$ particles is also determined by EDX (Supporting Information, Figure S3), and the atom ratio of Pd/Au in the alloy particles is 33:67, which is in line with the ratio detected by XRD and the concentration ratio in the electrodeposition solution.

3.3 Electrochemical Characterization

Figure 3 presents the cyclic voltammograms of different electrodes in $[Fe(CN)_6]^{3-/4-}$ solutions. As can be seen, $[Fe(CN)_6]^{3-/4-}$ exhibits a pair of small peaks at the GO/GCE and its blank current is also small, indicating that the electron-transfer rate of exfoliated GO is slower due to its poor conductivity. Moreover, the surface charges of the exfoliated GO repel the access of $[Fe(CN)_6]^{3-/4-}$ ions to the electrode surface for electrochemical reaction [23]. When IL is conjunct with GO, the peak current increases. This is due to the high electrical conductivity and masking effect of IL. After GO is electrochemically reduced to EGN, the peak current increases notably, which can be attributed to the high electrical conductivity of EGN, in addition to the decrease in electrostatic repulsion. When EGN is functionalized by IL the peaks of $[Fe(CN)_6]^{3-/4-}$ ions are bigger. This is related to the improved dispersion of EGN and the good electrical conductivity of IL. After the electrodeposition of PdAu alloy nanoparticles, the peak currents increase further, confirming the contribution of alloy nanoparticles in increasing the electroactive surface area and/or promoting the electron transfer [34].

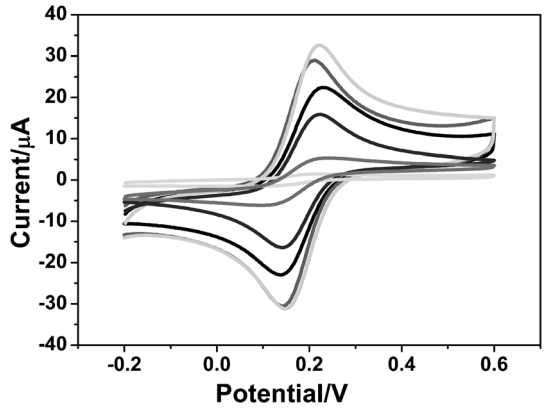

Fig. 3. Cyclic voltammograms of GO/GCE, GO-IL/GCE, GCE, EGN/GCE, EGN-IL/GCE, and $PdAu_2$-EGN-IL/GCE (from inner to outer) in 0.2 M KCl aqueous solution containing 5 mM $Fe(CN)_6^{3-/4-}$. Scan rate: 50 mV/s.

3.4 Comparison of the Electrochemical Oxidation of OA at Different Electrodes

The cyclic voltammograms of OA at different electrodes are compared in Figure 4. As can be seen, OA produces a very small peak at the bare GCE, implying that the electron-transfer of OA is quite slow at the electrode. When the GCE is coated with EGN the oxidation current of OA increases. At the EGN-IL/GCE OA exhibits a bigger anodic peak, meaning EGN and IL show cooperative action in promoting the electrooxidation of OA. As shown in Figure 4B, Pd-EGN-IL/GCE does not produce redox peaks in the potential range because of the formation of the oxide species of Pd [12]. Differently, the Au-EGN-IL/GCE and $PdAu_2$-EGN-IL/GCE present a wide anodic peak and a sharp cathodic peak, resulting from the redox of Au. When OA is present a distinct anodic peak occurs. Its peak potential is lower in comparison with that at a bare GCE. This indicates that the metal nanoparticles have catalysis to the electrochemical oxidation of OA. The catalytic oxidation of OA at Pd was thought to be associated with the electrochemical oxidation of Pd [12]:

$$Pd \rightarrow Pd^{II} + 2e$$

$$H_2C_2O_4 + Pd^{II} \rightarrow Pd + 2CO_2 + 2H^+$$

In this case, the oxidation mechanism of OA at AuPd-EGN-IL/GCE is thought to be similar to that at Pd-EGN-IL/GCE. At the $PdAu_2$-EGN-IL/GCE the OA peak is higher. This means that $PdAu_2$ alloy has superior electrocatalysis toward OA to monometal, due to the synergistic effect of different metals. Such phenomenon was also reported in literature [34].

The cyclic voltammograms of OA at $PdAu_2$/GCE, $PdAu_2$-EGN/GCE and $PdAu_2$-EGN-IL/GCE are presented in Figure 4C. Obviously, OA produces higher peak at the $PdAu_2$-EGN-IL/GCE. The reason is that more alloy nanoparticles are electrodeposited on the EGN-IL and the $PdAu_2$-EGN-IL/GCE has larger electrode area.

The response of OA at the $PdAu_2$–EGN-IL/GCE is also dependent on the bimetallic composition (Supporting Information, Figure S4). The peak current gradually increases with the $c(PdCl_2)/c(HAuCl_4)$ ratio changing from 10:0 to 1:2. However, when the ratio is further decreased, the peak current declines. Thus, the ratio of $c(PdCl_2)/c(HAuCl_4)$ is fixed at 1:2.

The electrodeposition time is another important factor influencing the electrochemical response of $PdAu_2$–EGN-IL/GCE to OA, and it is also optimized for OA sensing (Supporting Information, Fig. S4). When the electrodepo-

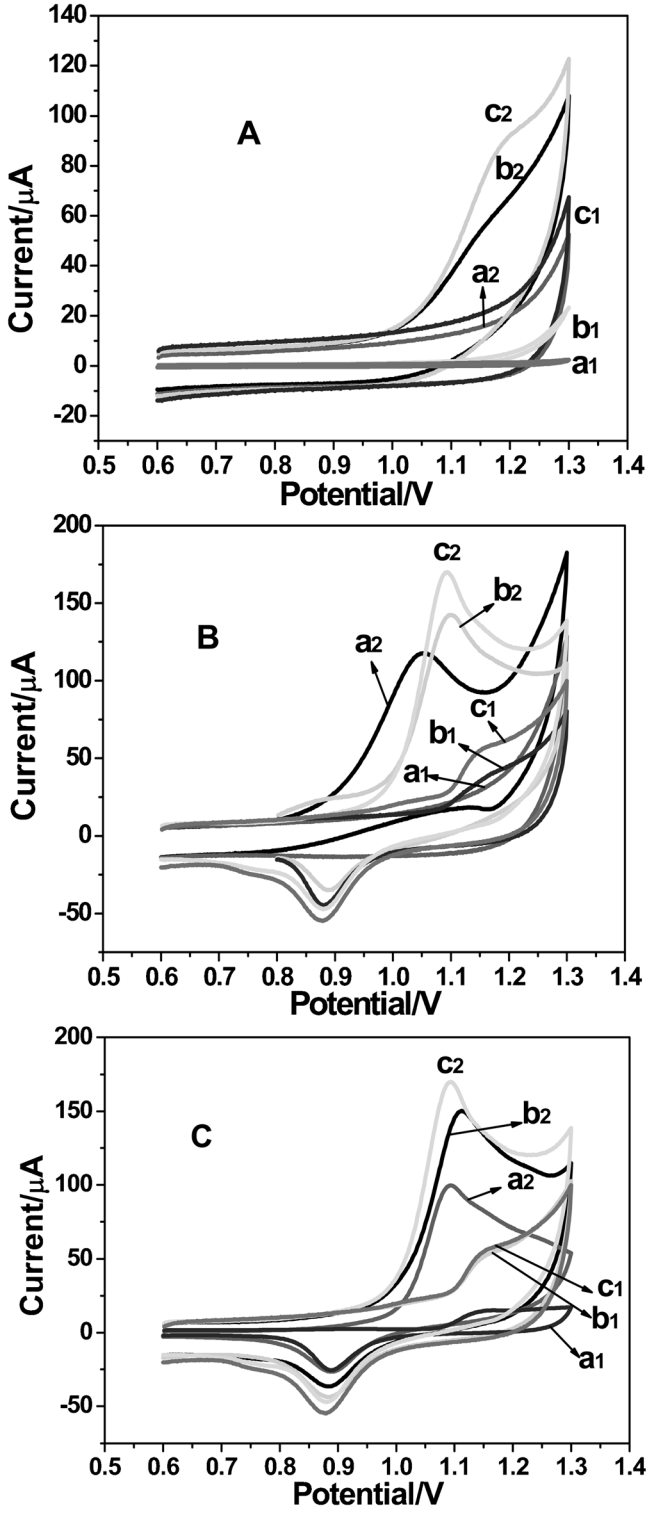

Fig. 4. (A) Cyclic voltammograms of bare GCE (a_1, a_2), EGN/GCE (b_1, b_2), and EGN-IL/GCE (c_1, c_2) in 0.2 M H_2SO_4 solution containing 0 mM (a_1, b_1, c_1) or 5 mM (a_2, b_2, c_2) OA. (B) Cyclic voltammograms of Pd-EGN-IL/GCE (a_1, a_2), Au-EGN-IL/GCE (b_1, b_2), and $PdAu_2$-EGN-IL/GCE (c_1, c_2) in 0.2 M H_2SO_4 solution containing 0 mM (a_1, b_1, c_1) or 5 mM (a_2, b_2, c_2) OA. (C) Cyclic voltammograms of $PdAu_2$/GCE (a_1, a_2), $PdAu_2$-EGN/GCE (b_1, b_2), and $PdAu_2$-EGN-IL/GCE (c_1, c_2) in 0.2 M H_2SO_4 solution containing 0 mM (a_1, b_1, c_1) or 5 mM (a_2, b_2, c_2) OA. Scan rate: 100 mV/s.

sition time is 200 s, OA exhibits bigger peak at the obtained $PdAu_2$-EGN-IL/GCE electrode. When the electrodeposition time is shorter, the density of alloy nanoparticle is lower, while a longer electrodeposition time leads to the aggregation of alloy nanoparticles, thus the alloy area and current response are smaller.

In addition, the influence of scan rate (v) is investigated from 20 mV/s to 200 mV/s (Supporting Information, Figure S5). As a result, the peak current and $v^{1/2}$ show a linear relationship, i_p (μA) = −13.8 + 14.1 $v^{1/2}$ (v: mV/s, R = 0.999) (Supporting Information, Figure S5). This indicates that the electrochemical process is diffusion-controlled. Meanwhile, the peak moves with changing scan rate. Furthermore, the peak potential and ln v show a linear relationship as E_{pa} (V) = 1.01 + 0.019 ln v. For an irreversible system the peak potential and scan rate should obey the following equation [35]:

$$E_{pa} = E^{\circ\prime} + m\,[0.78 + \ln\,(D_0^{1/2}/k_0) - 0.5\ln m] + (m/2)\,\ln v,\; m = RT/[(1-\alpha)\,n_\alpha\,F]$$

Logically, in this case 0.5 $RT/[(1-\alpha)\ n_\alpha F]$ ln v = 0.019 ln v. Assuming α is 0.5 for the irreversible electrochemical reaction, thus n_α is calculated to be 2. This is in agreement with the mechanism mentioned above.

3.5 Voltammetric Measurement of OA

Under the selected conditions, the linear sweep voltammograms of a series of OA solutions are recorded. As the $PdAu_2$-EGN-IL/GCE can produce redox peaks in blank solutions (Figure 4B, c_1), and they overlap with the OA peak to some extent, the background current is deducted from the voltammograms. Figure 5 presents the voltammograms after deducting the background current. The

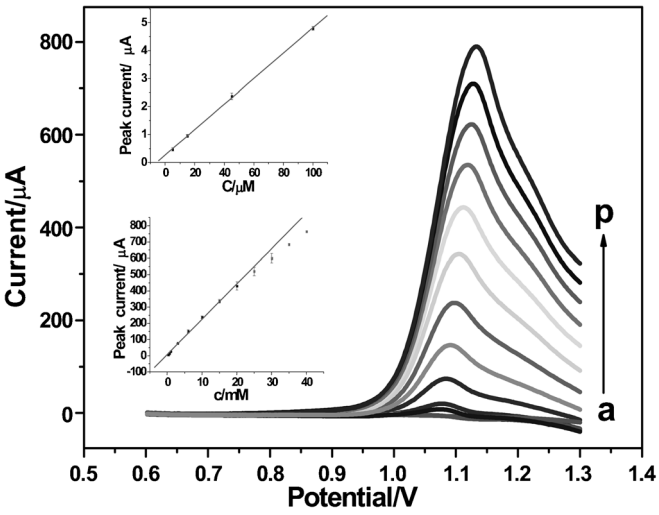

Fig. 5. Linear sweep voltammograms of OA at $PdAu_2$-EGN-IL/GCE after deducting the background current. OA concentration (from a to p): 0.005, 0.015, 0.045, 0.10, 0.30, 0.60, 1.0, 3.0, 6.0, 10.0, 15.0, 20.0, 25.0, 30.0, 35.0 and 40.0 mM. Scan rate: 100 mV/s; electrolyte: 0.2 M H_2SO_4. Inset: Calibration curves.

calibration curve for OA is linear in the range of 5 μM–0.1 mM and 0.3 mM–20 mM, with sensitivity of 45.5 μA/mM and 21.7 μA/mM, respectively; the detection limit is estimated to be 2.7 μM ($S/N=3$). In comparison with other electrodes or sensors, such as the exfoliated graphite–polystyrene composite electrode (with a detection limit of 0.05 mM and a linear range of 0.5–3 mM) [9], carbon nanotube modified electrode (with a detection limit of 12 μM) [10], SiO_2/SnO_2/CoPc–carbon paste modified electrode (with a detection limit of 7.1 μM) [11] and Pd-carbon nanofiber modified electrode (with a detection limit of 0.2 mM) [13], the $PdAu_2$–EGN-IL/GCE shows a lower detection limit and/or a wider linear range. The electrode also gives better performance than some other instrumental methods such as the spectrophotometry (with a detection limit of 19 μM and a linear range of 50–300 μM) [3] and the chromatography (with a detection limit of 6.2 μM and a linear range of 10 μM–4 mM) [4]. But its detection limit is higher than that of the enzymatic method (with a detection limit of 1 μM) [8].

3.6 Stability and Reproducibility of the $PdAu_2$–EGN-IL/GCE

To test the reproducibility and stability of the electrode, the response of 5 mM OA is recorded with seven electrodes prepared by the same way, and the relative standard deviation (*RSD*) of the peak current is 6.2%, indicating that the electrode is reproducible. Eight successive measurements using a $PdAu_2$-EGN-IL/GCE yield an *RSD* of 6.9%, indicating that the electrode can be used for the repeated detection of OA. The storage stability of the electrode is also examined. After a two-week store in a refrigerator, the response current retains 91% of its initial value. After one month it becomes 85%.

3.7 Application

In order to evaluate the practical feasibility of the proposed method for the determination of OA, the $PdAu_2$-EGN-IL/GCE electrode is applied to the determination of OA in spinach sample. The OA content in the spinach sample is calculated to be 3 mg/g in this case. Standard OA solutions are added to the sample solutions to estimate their recovery and it is 86–94% (Table 1). Here the recovery of standard OA solution added is calculated according to the OA concentration added and the OA concentration detected (i.e. the total concentration minus the original concentration 0.79 mM).

Table 1. Measurement results of OA in a spinach sample solution.

Sample	Added (mM)	Found (mM)	Recovery (%)
Spinach solution	0	0.79 ± 0.03	–
	1.0	1.65 ± 0.04	86
	2.5	3.2 ± 0.1	94
	5.0	5.5 ± 0.1	94
	7.5	7.7 ± 0.2	92

4 Conclusions

In summary, PdAu alloy nanoparticles can be prepared on an EGN-IL modified GCE by electrodeposition and the resulting $PdAu_2$-EGN-IL/GCE electrode exhibits strong electrocatalysis to the oxidation of OA in comparison with the corresponding monometal nanoparticle based electrodes (i.e. Au-EGN-IL/GCE and Pd-EGN-IL/GCE). Under the optimized conditions, the oxidation current of OA is linear to its concentration in a wide range and the detection limit is 2.7 μM ($S/N=3$). The electrode shows good stability and reproducibility and it can be used for the determination of OA content in real samples.

Acknowledgements

The Authors appreciate the financial support from the *National Natural Science Foundation of China* (Grant No.: 21075092), the *State Key Laboratory of Advanced Technology for Materials Synthesis and Processing* (*Wuhan University of Technology*, Grant No. 2010-KF-12), and the *State Key Laboratory of Electroanalytical Chemistry*, *Changchun Institute of Applied Chemistry*, *China*.

References

[1] P. R. Cheeke, *J. Anim. Sci.* **1995**, *73*, 909.
[2] P. Wescheebeling, R. Maiti, G. Garciadiaz, D. I. Gonzalez, F. Sosaalvarado, *Econ. Bot.* **1995**, *49*, 423.
[3] Q. Z. Zhai, X. X. Zhang, Q. Z. Liu, *Bull. Chem. Soc. Ethiopia* **2007**, *21*, 297.
[4] F. W. Wu, Z. K. He, Q. Y. Luo, Y. E. Zeng, *Food Chem.* **1999**, *65*, 543.
[5] D. J. Kim, H. Y. Kim, M. H. Kim, J. S. Lee, *Food Sci. Biotechnol.* **2007**, *16*, 650.
[6] L. Yang, L. Liu, B. A. Olsen, M. A. Nussbaum, *J. Pharm. Biomed. Anal.* **2000**, *22*, 487.
[7] E. F. Perez, G. D. O. Neto, *Sens. Actuators B* **2001**, *72*, 80.
[8] C. S. Pundir, N. Chauhan, Rajneesh, *Sens. Actuators B* **2011**, *155*, 796.
[9] F. Manea, C. Radovan, I. Corb, A. Pop, G. Burtica, P. Malchev, S. Picken, J. Schoonman, *Sensors* **2007**, *7*, 615.
[10] Y. Q. Zheng, C. Z. Yang, W. H. Pu, J. D. Zhang, *Food Chem.* **2009**, *114*, 1523.
[11] J. Arguello, H. A. Magosso, R. R. Ramos, T. C. Canevari, R. Landers, V. L. Pimentel, Y. Gushikem, *Electrochim. Acta* **2009**, *54*, 1948.
[12] I. G. Casella, *Electrochim. Acta* **1999**, *44*, 3353.
[13] Y. Liu, J. S. Huang, D. W. Wang, H. Q. Hou, T. Y. You, *Anal. Meth.* **2010**, *2*, 855.
[14] A. Berna, J. M. Delgado, J. M. Orts, A. Rodes, J. M. Feliu, *Langmuir* **2006**, *22*, 7192.
[15] J. Haber, P. Nowak, P. Zurek, *Langmuir* **2003**, *19*, 196.

[16] S. E. Habas, H. Lee, V. Radmilovic, G. A. Somorjai, P. Yang, *Nature* **2007**, *6*, 692.
[17] H. K. Chae, D. Y. Siberio-Perez, J. Kim, Y. Go, M. Eddaoudi, A. J. Matzger, M. O'Keeffe, O. M. Yaghi, *Nature* **2004**, *427*, 523.
[18] Y. B. Zhang, Y. W. Tan, H. L. Stormer, P. Kim, *Nature* **2005**, *438*, 201.
[19] C. S. Shan, H. F. Yang, D. X. Han, Q. X. Zhang, A. Ivaska, L. Niu, *Biosens. Bioelectron.* **2010**, *25*, 1070.
[20] J. J. Shi, J. J. Zhu, *Electrochim. Acta* **2011**, *56*, 6008.
[21] H. C. Gao, F. Xiao, C. B. Ching, H. W. Duan, *ACS Appl. Mater. Interf.* **2011**, *3*, 3049.
[22] Y. H. Song, Z. F. He, H. Z. Zhu, H. Q. Hou, L. Wang, *Electrochim. Acta* **2011**, *58*, 757.
[23] H. L. Guo, X. F. Wang, Q. Y. Qian, F. B. Wang, X. H. Xia, *ACS Nano* **2009**, *3*, 2653.
[24] Y. Y. Shao, J. Wang, M. Engelhard, C. M. Wang, Y. M. Lin, *J. Mater. Chem.* **2010**, *20*, 743.
[25] M. Zhou, Y. L. Wang, Y. M. Zhai, J. F. Zhai, W. Ren, F. Wang, S. J. Dong, *Chem. Eur. J.* **2009**, *15*, 6116.
[26] L. Y. Chen, Y. H. Tang, K. Wang, C. B. Liu, S. L. Luo, *Electrochem. Commun.* **2011**, *13*, 133.
[27] A. Safavi, A. R. Banazadeh, *Food Chem.* **2007**, *105*, 1106.
[28] H. J. Chen, S. J. Dong, *Langmuir* **2007**, *23*, 12503.
[29] C. X. Guo, Z. S. Lu, Y. Lei, C. M. Li, *Electrochem. Commun.* **2010**, *12*, 1237.
[30] Y. K. Yang, C. E. He, R. G. Peng, A. Baji, X. S. Du, Y. L. Huang, X. L. Xie, Y. W. Mai, *J. Mater. Chem.* **2012**, *22*, 5666.
[31] M. Acik, D. R. Dreyer, C. W. Bielawski, Y. J. Chabal, *J. Phys. Chem. C* **2012**, *116*, 7867.
[32] H. P. Klug, L. E. Alexander, in *X-ray Diffraction Procedures for Polycrystalline and Amorphous Materials*, 2nd ed., Wiley, New York **1974**.
[33] R. Jenkins, R. L. Snyder, *Introduction to X-Ray Powder Diffractometry*, Wiley, New York **1996**.
[34] J. Yang, S. Y. Deng, J. P. Lei, H. X. Ju, S. Gunasekaran, *Biosens. Bioelectron.* **2011**, *9*, 159.
[35] A. J. Bard, L. R. Faulkner, *Electrochemical Methods: Fundamentals and Applications*, JWiley, New York **1980**.

